Journal of Applied Physics

Phase dependence of Schottky barrier heights for Ge–Sb–Te and related phase-change materials

Cite as: J. Appl. Phys. **127**, 155301 (2020); https://doi.org/10.1063/5.0001912
Submitted: 21 January 2020 . Accepted: 01 April 2020 . Published Online: 15 April 2020

Zhaofu Zhang, Yuzheng Guo, and John Robertson

View Online

Export Citation

CrossMark

ARTICLES YOU MAY BE INTERESTED IN

Prediction of room-temperature multiferroicity in strained $MoCr_2S_6$ monolayer
Journal of Applied Physics **127**, 155302 (2020); https://doi.org/10.1063/1.5144535

Koopmans' tuning of HSE hybrid density functional for calculations of defects in semiconductors: A case study of carbon acceptor in GaN
Journal of Applied Physics **127**, 155701 (2020); https://doi.org/10.1063/1.5140661

Onset of ring defects in n-type Czochralski-grown silicon wafers
Journal of Applied Physics **127**, 153101 (2020); https://doi.org/10.1063/5.0005899

Lock-in Amplifiers up to 600 MHz

© 2020 Author(s).

Journal of Applied Physics ARTICLE scitation.org/journal/jap

Phase dependence of Schottky barrier heights for Ge–Sb–Te and related phase-change materials

Cite as: J. Appl. Phys. **127**, 155301 (2020); doi: 10.1063/5.0001912
Submitted: 21 January 2020 · Accepted: 1 April 2020 ·
Published Online: 15 April 2020

View Online

Export Citation

CrossMark

Zhaofu Zhang,[1] Yuzheng Guo,[2] and John Robertson[1,a)]

AFFILIATIONS

[1]Department of Engineering, University of Cambridge, Cambridge CB2 1PZ, United Kingdom
[2]College of Engineering, Swansea University, Swansea SA1 8EN, United Kingdom

[a)]**Author to whom correspondence should be addressed:** jr@eng.cam.ac.uk

ABSTRACT

The large difference of dielectric functions between the amorphous and crystalline phases of Ge–Sb–Te based phase-change materials (PCMs) used in memory storage devices also affects their Schottky barrier heights (SBHs) and thus their electrical device properties. Here, the SBHs of each phase of $Ge_2Sb_2Te_5$, GeTe, GeSe, and SnTe are found by density functional supercell calculations. The Fermi level pinning factor S calculated for the crystalline phases (with a larger dielectric constant) is smaller than their amorphous phases, agreeing well with the empirical relationship linking SBH to a dielectric constant. The relatively large dielectric constant of crystalline PCMs arises from their resonant bonding (metavalent bonding), but their pinning factor is not always as small as empirically expected. The results are useful for optimizing the design of metal contacts for Ge–Sb–Te type phase-change memory devices.

Published under license by AIP Publishing. https://doi.org/10.1063/5.0001912

I. INTRODUCTION

Phase-change materials (PCMs) based on Ge–Sb–Te chalcogenide alloys were initially developed for non-volatile optical storage disks.[1,2] These applications benefit from the superior properties of PCMs, such as extremely fast programming, excellent reliability, and easy downscaling. Their operation uses the rapid, reversible transition between their crystalline (c-) and amorphous (a-) phases. These phases had different optical properties due to the different primary bonding of each phase, particularly a strong contrast in their refractive indices n, due to the large n of the resonantly bonded or "metavalently bonded" crystalline phase.[3–6]

Unusually, the same materials are also the basis of non-volatile electronic memories,[7] the phase-change random access memories (PRAMs), where the different electrical resistivities are due to the different Fermi pinning energies (E_F) of the two phases, with E_F of c-PCMs pinned near the valence band maximum (VBM) giving it a much lower resistance. PRAM is now a leading contender for the storage class memory with a latency and costs between that of volatile dynamic random access memory (DRAM) and non-volatile flash memory.[7,8]

The future of PRAM depends to an extent on its continued dimensional scaling following Moore's law, and this in turn depends increasingly on the performance of its contacts. These are limited by the Schottky barrier heights (SBHs) of the contact metals with the phase-change semiconductor material. The SBHs also affect the carrier injection and leakage current in a PRAM array. The band line-ups of a-$Ge_2Sb_2Te_5$ with various dielectrics were studied sometime ago by photoemission.[9,10] The authors also reported metal contacts with a-$Ge_2Sb_2Te_5$, showing a pinning factor of 0.36–0.46.[11] However, only three metals were used, and the work only focused on the amorphous case. There has so far been no further analysis of the chemical trends of Ge–Sb–Te SBHs. Thus, a fundamental understanding of the Schottky barrier on different Ge–Sb–Te chalcogenides especially focusing on the effect of the phase on the barrier heights is still lacking, which is useful for the design of Ge–Sb–Te based memory devices.

The main chemical trends of the SBHs with the contact metal are defined by the semiconductor's charge neutrality level (CNL), and its slope factor $S = \partial\phi_p/\partial\Phi_M$, where ϕ_p is the p-type SBH and Φ_M is the metal work function of the contact.[12] The SBHs of semiconductors follow the equation[13]

$$S = \frac{1}{1 + \frac{e^2 N\delta}{\varepsilon\varepsilon_0}}, \tag{1}$$

Published under license by AIP Publishing.

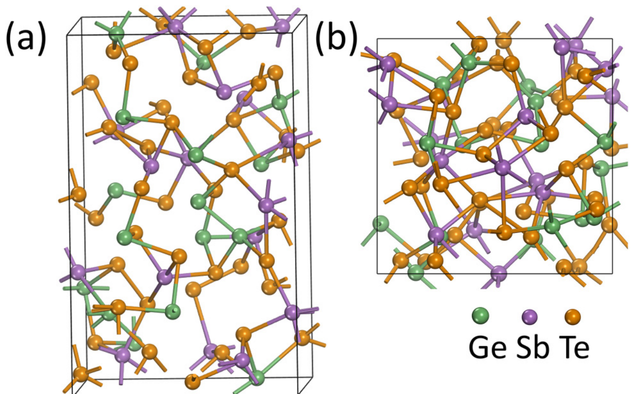

FIG. 1. (a) Side and (b) top view of amorphous $Ge_2Sb_2Te_5$. Green, purple, and brown balls are Ge, Sb, and Te atoms, respectively.

where N is the density of gap states at E_F causing the pinning, δ is their decay length, and ε is the dielectric constant of the interfacial layer. Generally, the pinning arises from metal-induced gap states (MIGS) caused by the metal contacts, which extend into the semiconductor bandgap. For a wide range of semiconductors and insulators, Schlüter[14] found that S tended to correlate with the optical dielectric constant ε_∞, and then Monch[15] observed an empirical model of SBH that S depends strongly on the optical dielectric constant of the semiconductor ($\varepsilon_\infty = n^2$), given by

$$S = \frac{1}{1 + 0.1(\varepsilon_\infty - 1)^2} \tag{2}$$

for a wide variety of semiconductors and insulators. Here, we discuss whether this interesting effect continues to the phase-change materials.

We note that the slope parameter S quantitatively characterizes the semiconductor pinning properties, with $S = 1$ describing no Fermi level pinning condition (Schottky limit) and $S = 0$ for the strong pinning case (Bardeen limit).[12,16] Thus, the ε_∞ values of each phase are very relevant not just to optical memories but also to the ultimate performance of electrical memory devices.

It should be noted that the appearance of ε_∞ in Eq. (2) does not mean that Schottky barriers (SBs) have optical functionalities. It means that S, N, and δ in Eq. (1) vary with parameters such as an average bandgap (Penn gap) and an MIGS decay length and overall tend to scale as in Eq. (2) for a wide range of materials with an octet of valence electrons.[17] Here, we extend this observation to non-octet materials with ten electrons. To do this, we compare calculated S values for differently bonded phases for various PCMs.

In this work, we calculate the SBHs of several Ge–Sb–Te type PCMs, including $Ge_2Sb_2Te_5$, GeTe, GeSe, and SnTe. Both crystalline and amorphous phases are investigated to compare the impact of different phases on their interface properties. The results show that the Ge–Sb–Te materials are all relatively strongly pinned with a Fermi level pinning factor S up to 0.3. For amorphous $Ge_2Sb_2Te_5$, the fitted pinning factor S agrees well with the previous experiment reports. Crystalline phases of Ge–Sb–Te all have obviously smaller S values (much stronger pinning effects) than the amorphous phases because of their different ε_∞ but not as small as empirically expected from Eq. (2). This may be because the role of metavalent bonding in empirical SBH models is not yet fully understood.

II. METHODS

The calculations were performed using the plane-wave CASTEP code.[18] We used norm-conserving pseudopotentials with a plane-wave cutoff energy of 500 eV and generalized gradient approximation (GGA) exchange-correlation functional. The effect of van der Waals's (vdW) interactions in these materials is included by the density functional theory (DFT)-D2 vdW correction via the Tkatchenko–Schefer scheme.[19,20] The supercell models are fully relaxed with a convergence tolerance of 10^{-5} eV for the total energy and 0.03 eV/Å for the force on each atom. In electronic calculations, the energy is converged to 10^{-6} eV/atom. The semi-local GGA functional narrows the semiconductor bandgap, as is well known, which increases the calculated ε_∞ values. The screened exchange (sX) hybrid functional[21] corrects the bandgap error where necessary, but sX is rather time-consuming and it is hard to converge for metallic contact systems. Therefore, only electronic

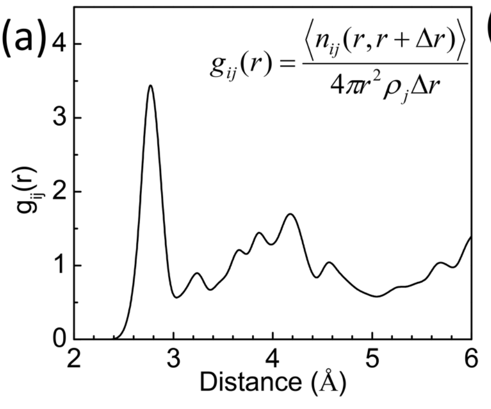

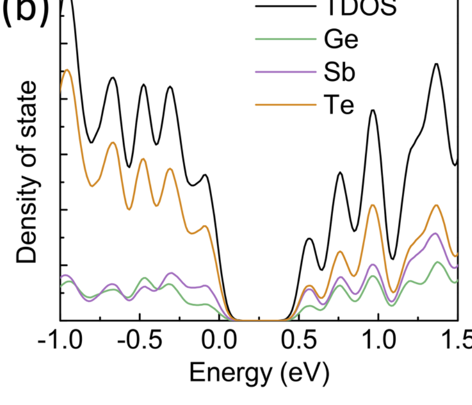

FIG. 2. (a) Averaged radial-distribution function curve, calculated with the inserted equation for the a-$Ge_2Sb_2Te_5$ model. (b) DOS of amorphous $Ge_2Sb_2Te_5$ by sX functional, showing a clean bandgap. The Fermi level is aligned at 0 eV.

Published under license by AIP Publishing.

TABLE I. Summary of the lattice constant and bandgap by PBE or sX functional calculations. Some experimental bandgaps are listed for reference.

Ge–Sb–Te PCMs		Lattice constant (Å)	PBE gap (eV)	sX gap (eV)	Exp. gap (eV)
$Ge_2Sb_2Te_5$	Mat-GST	a = b = 8.34	0.002	0.13	0.48[a] (Ref. 3)
	a-GST	…	0.32	0.51	0.77[3]
GeTe	r-GeTe	a = b = 4.13	0.47	0.57	0.55[3]
	o-GeTe	a = 4.20 b = 4.64	0.42	0.64	0.78[3]
GeSe	r-GeSe	a = b = 3.97	0.46	0.60	…
	o-GeSe	a = 4.02 b = 4.10	0.71	0.96	1.07[32]
SnTe	r-SnTe	a = b = 4.36	0.25	0.44	0.2,[33] 0.3[b] (Ref. 34)
	o-SnTe	a = 4.32 b = 4.58	0.80	1.01	…

[a]Experimental gap of c-$Ge_2Sb_2Te_5$ is from the rock-salt phase of $Ge_2Sb_2Te_5$.
[b]Experimental gap of SnTe is from cubic SnTe.

structures and optical dielectric functions of bulk materials are calculated by sX. Note that our work focuses on SBH changes (i.e., the slope) with the metal work function, which are less affected by absolute bandgap values. Lattice matching at the interfaces between the metal and semiconductors was achieved by rotating the lattices where necessary. The metal slabs were adjusted to contain an even number of electrons to give spinless systems.

For GeTe, GeSe, and SnTe, the high-symmetry rhombohedral (r-) and low-symmetry orthorhombic (o-) structures are used to represent the crystalline and amorphous phases, respectively.[5,22] o-GeTe has been proposed previously as a simple model of bonding in amorphous GeTe,[5] which loses the medium-range order and alignment of *p*-orbitals found in r-GeTe, while keeping the same coordination number. That is, there is no metavalent bonding in the o-phases. For $Ge_2Sb_2Te_5$, the c-phase was taken from the mixed $Ge_2Sb_2Te_5$ structure of Matsunaga,[23] which is a 50% mixed chalcogenide super-lattice (CSL) structure with a mirror symmetry and has lower energy than the Kooi structure.[24,25] The chalcogenide superlattice, or the interfacial phase-change memory (iPCM), consists of a hexagonal $(GeTe)_n(Sb_2Te_3)_m$ layer,

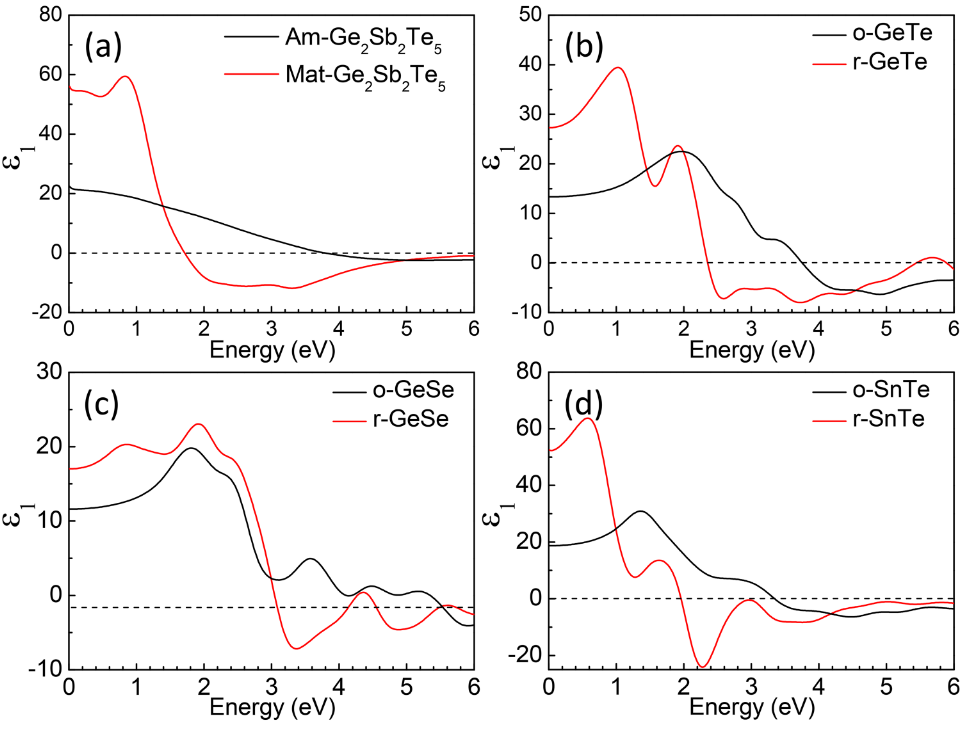

FIG. 3. Calculated dielectric constant real part ε_1 for (a) $Ge_2Sb_2Te_5$, (b) GeTe, (c) GeSe, and (d) SnTe by sX functional. The black and red lines represent the amorphous and crystalline phases, respectively. The c-$Ge_2Sb_2Te_5$ is taken to have the Matsunaga-mixed CSL structure,[23] labeled "Mat" in (a).

Published under license by AIP Publishing.

TABLE II. Summary of the dielectric constant and pinning factor by different methods. The CNL position is the energy position above the VBM.

Ge–Sb–Te PCMs		sX ε_1	Exp. ε_1	S (Monch's with sX ε_1)	S (supercell model)	S (exp. report)	CNL (eV) (supercell model)
$Ge_2Sb_2Te_5$	Mat-GST	56.0	33.3[a] (Ref. 3)	0.0033	~0.15	…	0.08
	a-GST	22.3	16.0[3]	0.021	~0.30	0.36–0.46[11]	0.34
GeTe	r-GeTe	27.3	33.2[3]	0.014	~0.04	…	0.30
	o-GeTe	13.3	13.2[3]	0.062	~0.29	…	0.74
GeSe	r-GeSe	17.0	24.5[b] (Ref. 6)	0.038	~0.08	…	0.39
	o-GeSe	11.6	13.5[6]	0.082	~0.37	…	0.99
SnTe	r-SnTe	52.5	~50[32]	0.0038	~0.05	…	0.09
	o-SnTe	18.7	…	0.031	~0.15	…	0.70

[a]Experimental ε_1 of c-$Ge_2Sb_2Te_5$ is the rock-salt type of $Ge_2Sb_2Te_5$.
[b]Experimental ε_1 of r-GeSe is from r-$GeSe_{0.75}Te_{0.25}$.

where the phase transition is constrained to move in one dimension rather than three dimensions so that less energy is consumed than the classical transition.[26] The random network of a-$Ge_2Sb_2Te_5$ was generated by molecular dynamics as we did previously.[22] During the molecular dynamics process, the experimental mass density of 5.87 g/cm^3 was kept.[27]

The SBHs are calculated using supercell models consisting of a- or c-phase semiconducting PCMs with a metal slab on top. A 15 Å thick vacuum layer is added to this to avoid the image effects. The electron affinity of a-Ge2Sb2Te5 is found to be 4.76 eV, close to its experimental value.[28] Re, Rh, Pd, Ir, and Pt contact metals are used for $Ge_2Sb_2Te_5$ as these are compatible with its electron affinity, while more metals are used for other PCMs, which have relatively lower electron affinity values. The high work function oxide MoO_3 is used where necessary to extend the range of work functions.[29]

III. RESULTS

The crystal $Ge_2Sb_2Te_5$, either the rock-salt structure or the CSL structure,[25] has ordered bonding. The Ge, Sb, and Te sites all have three shorter bonds and three longer bonds, as found experimentally.[30] After molecular dynamics, the Ge coordination falls to four, and the final a-$Ge_2Sb_2Te_5$ mainly has the Ge–Te and Sb–Te bonding character with negligible Ge–Sb and Ge–Ge bonds [Figs. 1(a) and 1(b)].

The radial-distribution function (RDF) curve in Fig. 2(a) features an averaged bond length of 2.75 Å and some moderately long interaction distances of up to 2.95 Å. The amorphous bonding characteristics are consistent with these reports.[31] Table I summarizes the lattice constant and calculated bandgap values for all studied Ge–Sb–Te PCMs.

A clean bandgap of 0.5 eV is observed by an sX hybrid functional calculation, as shown in Fig. 2(b). The partial density of states (PDOS) shows that the VBM is mainly localized on the Te-states, whereas the conduction band minimum has a mixture of Sb and Te states. Table I summarizes the lattice constant and calculated bandgap values for all studied Ge–Sb–Te PCMs.

The calculated real part ε_1 of optical dielectric functions for the c- and a-phases of PCMs is shown in Fig. 3. A much larger ε_1 value for the c-phase (red line) compared with the a-phase (black line) can be observed, agreeing with experimental values[3] and previous calculations.[5] The p-orbital alignment in the resonantly bonded c-phase of $Ge_2Sb_2Te_5$, GeTe, and SnTe leads to

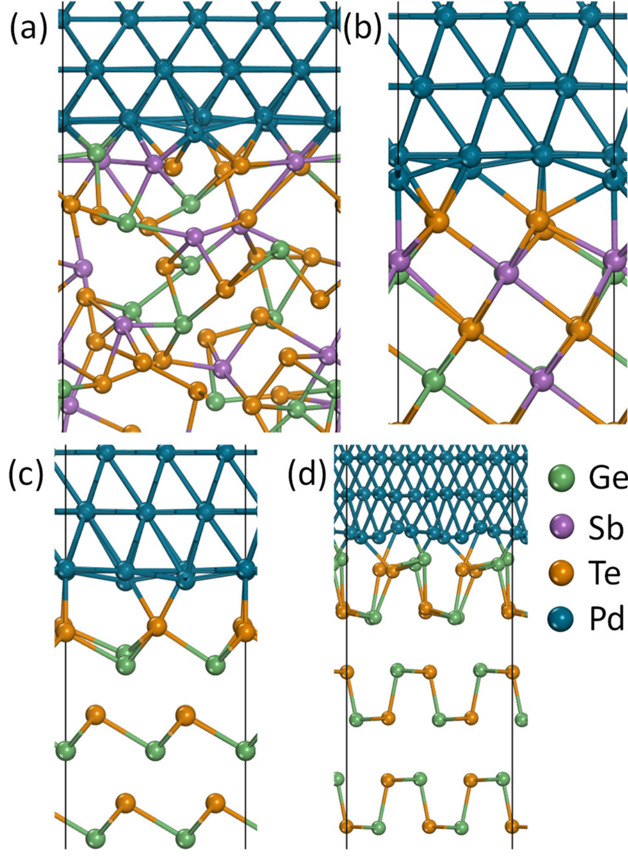

FIG. 4. Atomic interface structures of (a) a-$Ge_2Sb_2Te_5$, (b) Matsunaga-mixed $Ge_2Sb_2Te_5$, (c) r-GeTe, and (d) o-GeTe with the Pd metal slab on top.

Published under license by AIP Publishing.

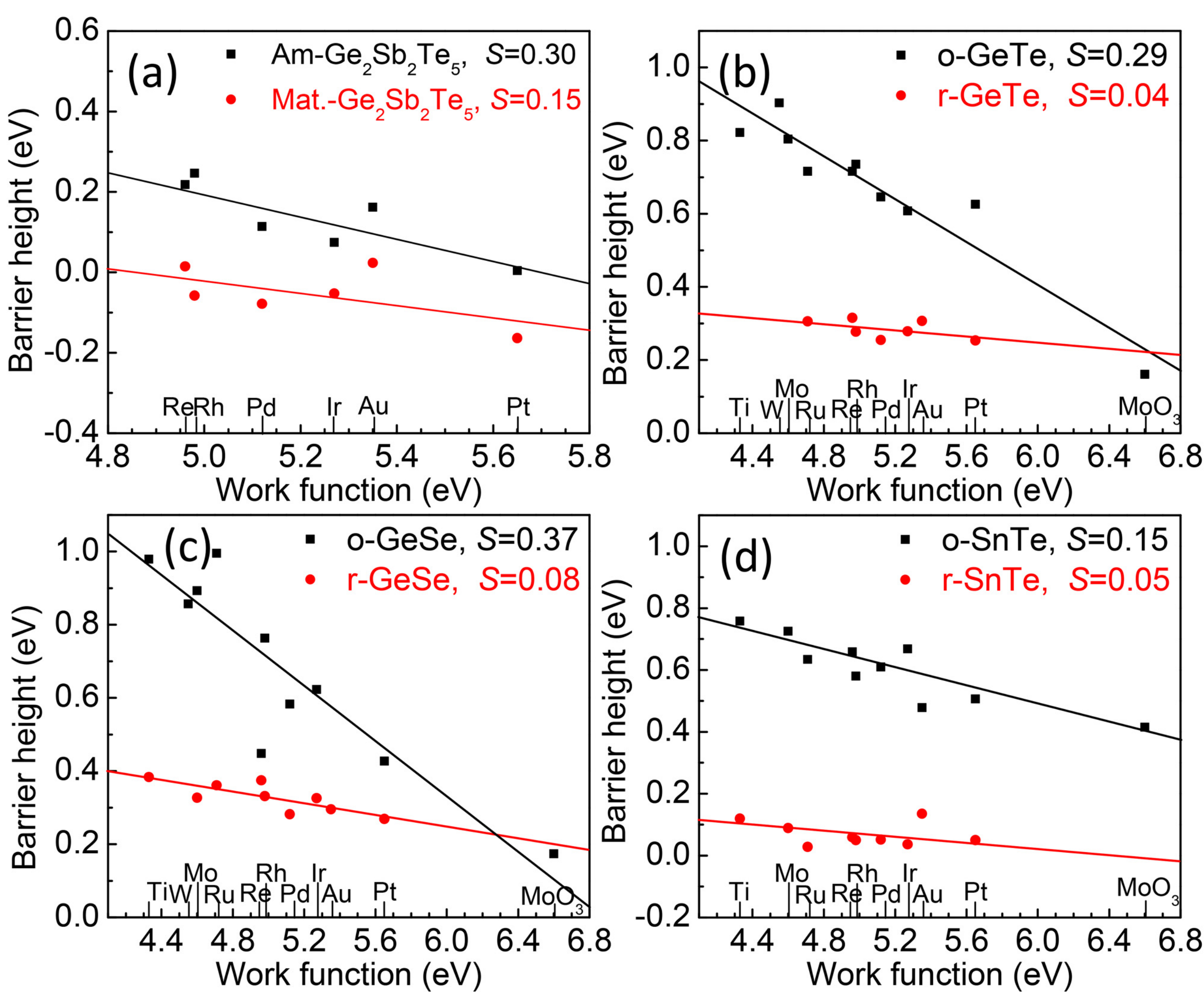

FIG. 5. *p*-type SBHs with different contact metals for (a) $Ge_2Sb_2Te_5$, (b) GeTe, (c) GeSe, and (d) SnTe. Both a- and c-phases are considered. For the r-phases, the SBH values are averaged values for Ge-terminated and chalcogen-terminated polar interfaces.

larger optical matrix elements for this phase, leading to their greater ε_∞ values.[5] For GeSe, the optical contrast is weaker than that of GeTe but still features a 1.5 times difference in $\varepsilon_1(0)$. A detailed comparison of dielectric constants is summarized in Table II.

The Schottky barrier height values are obtained from the metal/PCM supercell models. Several interface models are shown in Fig. 4. Note that GeSe and SnTe in our calculation have the same symmetries as GeTe and thus similar interface supercells. For a-GST, the disordered bonding character enables metal atoms to bond to Ge, Sb, or Te atoms at the interface. After relaxation, the interfacial Ge–Sb–Te sites bond with metal atoms, causing a local distortion. However, the local distortion decays when the atoms lie farther from the interface and almost disappears in the third atomic layer as shown in Fig. 4. Our thick PCM slabs (~10 layers) guarantee the bulk bonding character and band structures for atoms in the interface supercells.

The *p*-type SBH is the energy difference between the VBM and metal Fermi level E_F. The Schottky barrier height can be derived using the core-level line-up scheme,[35] expressed by

$$\Phi_p = E_{core}^{interface} + \Delta V - E_F, \quad (3)$$

where $E_{core}^{interface}$ is the core-level state position of bulk atoms in the interface supercell and ΔV is the energy difference of the bulk VBM and the bulk core-level state.[29]

Published under license by AIP Publishing.

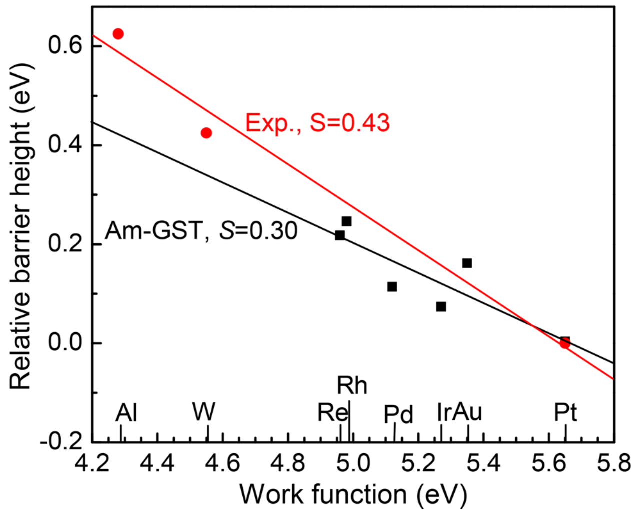

FIG. 6. SBH comparison between calculations and an experimental report.[11] The experimental SBHs are shifted with Pt's SBH aligned to 0, to have a compatible comparison with the calculation data.

The calculated SBH distributions as a function of the metal work function for crystalline and amorphous supercell models are shown in Fig. 5, where SBH values for r-GeTe, etc., are averaged values for Ge-terminated and chalcogen-terminated polar interfaces. Several apparent phenomena can be observed. Firstly, the barrier heights all decrease linearly with the increased metal work function. The S for the Matsunaga-$Ge_2Sb_2Te_5$ structure is ~0.15. However, a larger S (0.28) occurs for a-$Ge_2Sb_2Te_5$, indicating relatively weaker pinning. A similar tendency also suits GeTe, GeSe, and SnTe models where a smaller slope is observed for the c-phase. For GeTe, GeSe, and SnTe, the a-phase PCMs have a slope of ~0.15–0.35, but their c-phases have an extremely strong pinning effect with $S < 0.1$ with excellent linearity. Apart from the slope contrast, the SBH values for a-PCMs are obviously larger than their crystalline counterparts, due to their smaller ε_∞.

The contrast of the fitted slope between the amorphous and crystalline materials in Fig. 5 arises from their different ε_∞ according to Eq. (2), and the physical explanation lies in the metavalent bonding of crystalline phases.[5] Table II summarizes the dielectric constant and the Fermi level pinning factors by different schemes. Our sX calculation reproduces well the experimental optical dielectric functions. A <0.05 S value is expected if taking either our calculated or experimental dielectric constant into Eq. (2). However, our fitted S values from supercell models are several times (even ~2 orders for $Ge_2Sb_2Te_5$) larger than the empirical ones, indicating that the empirical SBH theory may be less applicable for the metavalently bonded semiconductors so far and that a deeper understanding of Schottky barriers in such systems is still needed. The only experiment report of different metals on Ge–Sb–Te type PCMs gives a moderate S value of 0.36–0.46[11] for amorphous $Ge_2Sb_2Te_5$, close to our calculated value of ~0.30 (Fig. 6). However, Fang *et al.*[11] obtained unusual negative SBH values from XPS data; these values should be confirmed by electrical measurements.

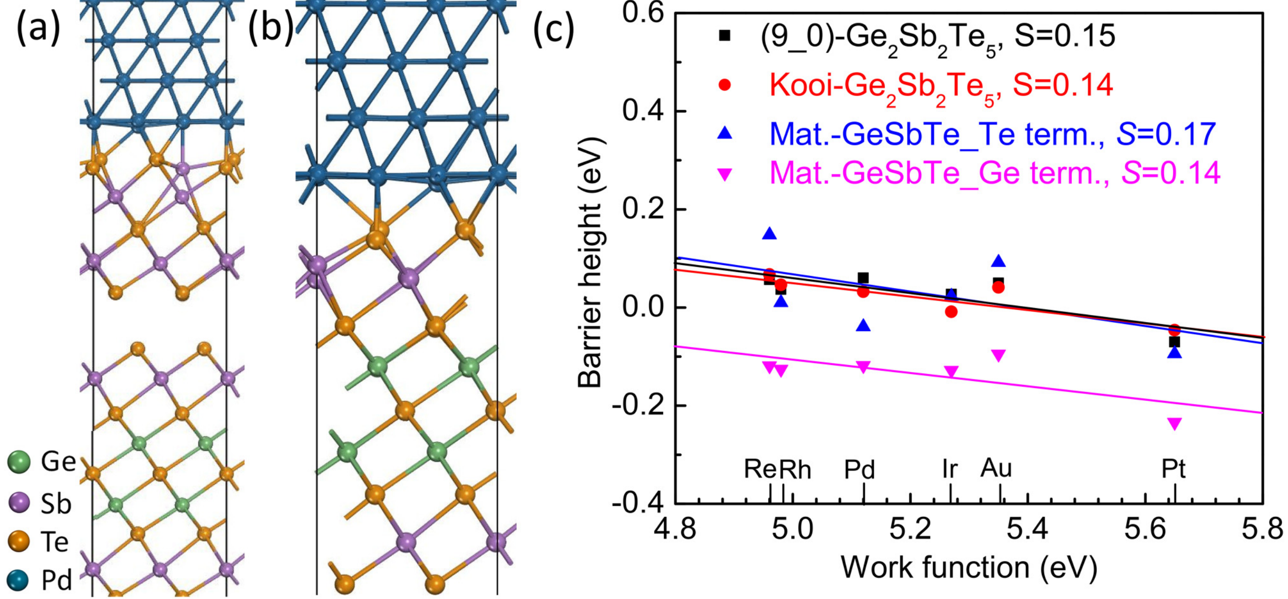

FIG. 7. Atomic structure for (a) (9_0)- and (b) Kooi-$Ge_2Sb_2Te_5$ with the Pd metal slab on top. (c) *p*-type SBHs with contact metals for several crystalline $Ge_2Sb_2Te_5$. Different faces of Matsunaga-GeSbTe with Ge-termination and Te-termination are presented, respectively.

Published under license by AIP Publishing.

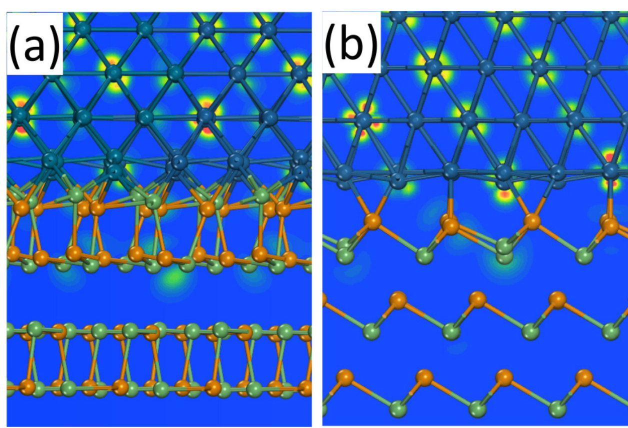

FIG. 8. Wave functions for bands across the Fermi level for (a) o-GeTe and (b) r-GeTe interface models, respectively.

Apart from this, as for c-$Ge_2Sb_2Te_5$, several other crystalline superlattice configurations are also calculated to show how the SBH varies with different faces, shown in Fig. 7. We see how a Ge- or Te-termination produces an offset of the SBH values, while the calculated slope factors (S values) for each of the faces are roughly the same within 0.1–0.2. The (9_0)-$Ge_2Sb_2Te_5$ and Kooi-$Ge_2Sb_2Te_5$ in Figs. 7(a) and 7(b) are another two kinds of CSL structures and are taken from Ref. 25.

Thus, our supercell calculation results are reliable enough to evaluate the Schottky contact behavior of Ge–Sb–Te PCMs. Taking the fitted S and the calculated bandgap and affinity into consideration, the CNL values (above VBM) can be extracted from fitted S data, using[12,16]

$$\Phi_n = (E_{CNL} - \chi) + S(\Phi_M - E_{CNL}). \tag{4}$$

The CNL data are summarized in Table II. Clearly, the CNL levels for c-PCMs lie closer to the VBM than for the amorphous cases, leading to much lower resistance for PRAM devices. The low CNL near the VBM results in a lower hole barrier because the metal Fermi levels tend to pin at CNL, which is important for current transport across the interface. This also indicates that E_F does not necessarily pin by defects, as is often said.

The technological consequences are that the moderate S value for a-PCMs allows its SBH to be tuned by changing the contact metal, which is useful for reasonable designs of PRAM devices. On the other hand, the very small (or even negative for c-$Ge_2Sb_2Te_5$) SBHs in Fig. 4 for c-PCMs mean that metal Fermi levels lie close to (or in) the valence band; therefore, they are actually ohmic contacts. Thus, the c-phase PCMs are actually heavily p-type semiconductors with low contact resistances, and the practical barrier height variation by changing the metal work function is small. These results are instructive for the reasonable design of the Ge–Sb–Te material interface contacts.

Figure 8 shows the orbital wave functions around the Fermi level for amorphous and crystalline GeTe supercell models. Apparently, the wave functions mainly distribute within the metal, but some states still decay into the semiconductor side, indicating that metal-induced gap states (MIGS)[12,16] exist. However, the decay length is limited and obviously shorter in PCM than in the classical semiconductor,[36] further confirming that the traditional SBH theory is less applicable to such semiconductors so far and further theoretical work is required.

IV. CONCLUSIONS

In conclusion, the Schottky barrier heights of metal/Ge–Sb–Te based phase-change material supercells are studied. We found that the Ge–Sb–Te materials have a relatively strong Fermi level pinning effect with pinning factor $S < 0.3$ for all kinds of phases. The crystalline Ge–Sb–Te chalcogenides have a much smaller S value compared with the amorphous counterparts, indicating stronger pinning effects. However, the S value is not as small as empirically expected, due to its crystalline metavalent bonding characteristics.

ACKNOWLEDGMENTS

We acknowledge the financial support from the European Union's Horizon 2020 research and innovation program PHASECHANGE SWITCH (No. 737109) and the support from Supercomputing Wales under Project No. SCW1070.

REFERENCES

[1]N. Yamada, E. Ohno, N. Akahira, K. Nishiuchi, K. Nagata, and M. Takao, Jpn. J. Appl. Phys. **26**, 61 (1987).
[2]D. Lencer, M. Salinga, and M. Wuttig, Adv. Mater. **23**, 2030 (2011).
[3]K. Shportko, S. Kremers, M. Woda, D. Lencer, J. Robertson, and M. Wuttig, Nat. Mater. **7**, 653 (2008).
[4]M. Wuttig and N. Yamada, Nat. Mater. **6**, 824 (2007).
[5]B. Huang and J. Robertson, Phys. Rev. B **81**, 081204 (2010).
[6]M. Zhu, O. Cojocaru-Mirédin, A. M. Mio, J. Keutgen, M. Küpers, Y. Yu, J. Cho, R. Dronskowski, and M. Wuttig, Adv. Mater. **30**, 1706735 (2018).
[7]S. Raoux, W. Wełnic, and D. Ielmini, Chem. Rev. **110**, 240 (2010).
[8]W. Zhang, R. Mazzarello, M. Wuttig, and E. Ma, Nat. Rev. Mater. **4**, 150 (2019).
[9]L. W. Fang, J. Pan, R. Zhao, L. Shi, T. Chong, G. Samudra, and Y. Yeo, Appl. Phys. Lett. **92**, 032107 (2008).
[10]J. Pan, L. W. Fang, Z. Zhang, and Y. Yeo, Surf. Interface Anal. **44**, 1013 (2012).
[11]L. W. Fang, Z. Zhang, R. Zhao, J. Pan, M. Li, L. Shi, T. Chong, and Y. Yeo, J. Appl. Phys. **108**, 053708 (2010).
[12]J. Robertson, J. Vac. Sci. Technol. B **18**, 1785 (2000).
[13]A. M. Cowley and S. M. Sze, J. Appl. Phys. **36**, 3212 (1965).
[14]M. Schlüter, Phys. Rev. B **17**, 5044 (1978).
[15]W. Monch, Phys. Rev. Lett. **58**, 1260 (1987).
[16]J. Robertson, J. Vac. Sci. Technol. A **31**, 050821 (2013).
[17]W. Mönch, Appl. Surf. Sci. **92**, 367 (1996).
[18]S. J. Clark, M. D. Segall, C. J. Pickard, P. J. Hasnip, M. J. Probert, K. Refson, and M. C. Payne, Z. Kristallogr. **220**, 567 (2005).
[19]A. Tkatchenko and M. Scheffler, Phys. Rev. Lett. **102**, 073005 (2009).
[20]T. Bučko, S. Lebègue, J. Hafner, and J. G. Ángyán, Phys. Rev. B **87**, 064110 (2013).
[21]S. J. Clark and J. Robertson, Phys. Rev. B **82**, 085208 (2010).
[22]B. Huang and J. Robertson, Phys. Rev. B **85**, 125305 (2012).
[23]T. Matsunaga, N. Yamada, and Y. Kubota, Acta Cryst. B **60**, 685 (2004).
[24]G. C. Sosso, S. Caravati, C. Gatti, S. Assoni, and M. Bernasconi, J. Phys. Condens. Matter **21**, 245401 (2009).

Published under license by AIP Publishing.

[25] X. Yu and J. Robertson, Sci. Rep. **5**, 12612 (2015); X. Yu and J. Robertson, Sci. Rep. **6**, 37325 (2016).
[26] R. E. Simpson, P. Fons, A. V. Kolobov, T. Fukaya, M. Krbal, T. Yagi, and J. Tominaga, Nat. Nanotechnol. **6**, 501 (2011).
[27] W. K. Njoroge, H. Wöltgens, and M. Wuttig, J. Vac. Sci. Technol. A **20**, 230 (2002).
[28] H. Tong, Z. Yang, N. N. Yu, L. J. Zhou, and X. S. Miao, Appl. Phys. Lett. **107**, 082101 (2015).
[29] Y. Guo, D. Liu, and J. Robertson, ACS Appl. Mater. Interfaces **7**, 25709 (2015).
[30] A. V. Kolobov, P. Fons, A. I. Frenkel, A. L. Ankudinov, J. Tominaga, and T. Uruga, Nat. Mater. **3**, 703 (2004).
[31] M. Xu, Y. Q. Cheng, H. W. Sheng, and E. Ma, Phys. Rev. Lett. **103**, 195502 (2009).
[32] R. Eymard and A. Otto, Phys. Rev. B **16**, 1616 (1977); N. Suzuki, and S. Adachi, Jpn. J. Appl. Phys. **34**, 5977 (1995).
[33] Z. V. Borges, C. M. Poffo, J. C. D. Lima, S. M. D. Souza, D. M. Trichês, and R. S. D. Biasi, Mater. Res. **21**, e20171077 (2018).
[34] L. Esaki and P. J. Stiles, Phys. Rev. Lett. **16**, 1108 (1966).
[35] E. A. Kraut, R. W. Grant, J. R. Waldrop, and S. P. Kowalczyk, Phys. Rev. Lett. **44**, 1620 (1980).
[36] J. Chen, Z. Zhang, Y. Guo, and J. Robertson, Microelectron. Eng. **216**, 111056 (2019).

Published under license by AIP Publishing.